Yuan et al. *EPJ Quantum Technology* (2024) 11:2
https://doi.org/10.1140/epjqt/s40507-023-00212-y

EPJ Quantum Technology
a SpringerOpen Journal

RESEARCH **Open Access**

A Rydberg atom-based amplitude-modulated receiver using the dual-tone microwave field

Jinpeng Yuan[1,2*], Ting Jin[1,2], Yang Yan[1,2], Liantuan Xiao[1,2], Suotang Jia[1,2] and Lirong Wang[1,2*]

*Correspondence: yjp@sxu.edu.cn; wlr@sxu.edu.cn
[1]The State Key Laboratory of Quantum Optics and Quantum Optics Devices, Shanxi University, 92 Wucheng Road, Taiyuan, 037006, Shanxi Province, China
[2]Collaborative Innovation Center of Extreme Optics, Shanxi University, 92 Wucheng Road, Taiyuan, 037006, Shanxi Province, China

Abstract

We propose a Rydberg atom-based receiver for amplitude-modulation (AM) reception utilizing a dual-tone microwave field. The pseudo-random binary sequence (PRBS) signal is encoded in the basic microwave field (B-MW) at the frequency of 14.23 GHz. The signal can be decoded by the atomic receiver itself but more obvious with the introduction of an auxiliary microwave (A-MW) field. The receiver's amplitude variations corresponding to microwave field are simulated by solving density matrices to give this mechanism theoretical support. An appropriate AM frequency is obtained by optimizing the signal-to-noise ratio, guaranteeing both large data transfer capacity (DTC) and high fidelity of the receiver. The power of two MW fields, along with the B-MW field frequency, is studied to acquire larger DTC and wider operating bandwidth. Finally, the readout of PRBS signals is performed by both the proposed and conventional mechanisms, and the comparison proves the obvious increment of DTC with the proposed scheme. This proof-of-principle demonstration exhibits the potential of the dual-tone scheme and offers a novel pathway for Rydberg atom-based microwave communication, which is beneficial for long-distance communication and weak signal perception outside the laboratory.

Keywords: Rydberg atom; Atomic receiver; Amplitude-modulation; Microwave communication

1 Introduction

The Rydberg atom-based sensors have been seen growing interest for a range of applications in microwave sensing, metrology, and communication. The sensing accuracy is promoted owing to the large transition dipole moments and the long lifetime of Rydberg states [1–3]. The metrology standard is promised by self-calibration ability and International System of Units (SI)) traceability of inherently quantum mechanical [4, 5]. The communication efficiency is guaranteed by plentiful Rydberg levels and fast responses of the atomic ensemble [6, 7]. As a result, several applications have been demonstrated, including electric field probes [8–10], stereo collectors [11], spectrum analyzers [12], location system [13], and digital communication receivers responding to amplitude modulated (AM) [14–19], frequency modulated (FM) [11, 16], or phase modulated (PM) methods [20, 21].

Especially, optical readout methods based on electromagnetically induced transparency (EIT) and Aulter-Townes splitting (AT splitting) schemes of Rydberg atom-based receiver have unique communication advantages. Firstly, the Rydberg atom-based receiver reads modulated signals in real-time while do not require additional demodulation devices. The introduction of the atomic superheterodyne mechanism makes it possible to read out PM signals directly on the basis of the original AM and FM self-demodulation capabilities [8, 10, 11]. Secondly, the frequency intervals between Rydberg levels covering from megahertz to terahertz bands allow the small-sized Rydberg receivers to overcome the Chu limit in the conventional dipole antenna, avoiding electromagnetic interference and miniaturizing the whole device [5, 6]. Thirdly, the atomic species, Rydberg levels, and spatial positions provide various channels for multiplexing in one atomic vapor cell [22–26]. Therefore, multiple channels are ready for transferring different information and signals. Finally, the Rydberg atom-based receiver's robust dynamic range from nV/cm to V/cm scale has been confirmed, which refers to the strength ratio between the maximum and the minimum received signals without distortion [27, 28].

The Rydberg atom-based receiver's data transfer capacity (DTC) is one of key parameters to determine the achievable communication rate for a channel. Various mechanisms have been proposed to increase the DTC of Rydberg atom-based receivers. The near photon-shot-noise channel capacity limit is realized by the phase-sensitive conversion of AM-encoded microwave signals into optical signals [1]. The spatially distributed probe light beams are implemented as an array of atom-optical receivers, improving the DTC by increasing the number of channels [24]. On the other hand, new mechanisms are also explored to extend the parallel operating bandwidth of Rydberg atom-based receivers. The signals in the MHz band are demodulated by a three-photon excitation scheme with an off-resonant heterodyne method [29]. The Rydberg alternating current (AC) Stark's mechanism enables digital communication with operating carrier frequency continuously from 0.1 GHz to 5.0 GHz [30, 31]. Multiple resonant response profiles of a Rydberg atomic receiver are utilized to receive microwave with frequency ranging from 1.7 GHz to 116 GHz [32]. A deep-learning algorithm is introduced to encode and decode the frequency-division multiplexed signals [33]. However, the performance improvement of the Rydberg atom-based receivers still calls for development.

In this work, a Rydberg atom-based AM receiver utilizing a dual-tone microwave field is demonstrated. The basic microwave field (B-MW) field at a frequency of 14.23 GHz carries a pseudo-random binary sequence (PRBS) signal. The atomic receiver has self-demodulation capability, which is enhanced since the introduction of an auxiliary microwave (A-MW). The performance of the receiver is simulated under different microwave fields to obtain the optimal operating conditions. The appropriate and applicable AM frequency, which indicates both large DTC and high fidelity of the receiver, is obtained. The power of the two microwave fields, together with the B-MW field frequency, is investigated to acquire appropriate DTC and operating bandwidth. Finally, the transferred PRBS signals between the proposed and conventional mechanisms are compared to verify the increment of DTC. This work builds a new avenue for Rydberg atom-based microwave communication, which brings it one step closer to practical application.

2 Experimental setup

Figure 1(a) shows the relevant energy levels diagram of ^{85}Rb. The atoms are excited from the ground state $5S_{1/2}(F = 3)$ to the Rydberg state $53D_{5/2}$ by a two-photon transition. The

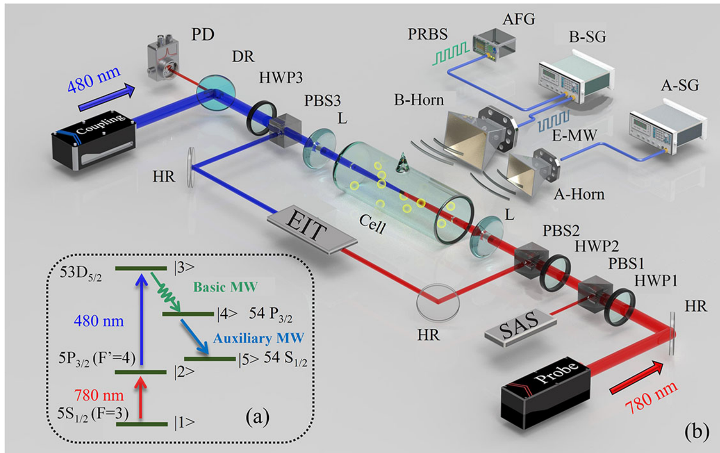

Figure 1 (a) The relevant energy levels diagram of ^{85}Rb. (b) The schematic of the experimental setup. PD, photodiode detector; HR, high reflective mirror; DM, dichroic mirror; HWP, half-wave plate; PBS, polarization beam splitter; L, lens; M, high reflection mirror; EIT, electromagnetically induced transparency spectroscopy; SAS, saturation absorption spectroscopy; Horn, horn antenna; SG, vector signal generator; AFG, arbitrary function generator; PRBS, pseudo-random binary sequence; E-MW, encoded microwave

transitions from the $53D_{5/2}$ state to two adjacent Rydberg states, $54P_{3/2}$ and $54S_{1/2}$, are stepwise excited by a 14.23 GHz B-MW field encoded through AM method and a constant 24.12 GHz A-MW field, respectively.

Figure 1(b) shows the schematic diagram of the experimental setup. The probe beam with a wavelength of 780 nm from an external cavity diode laser (DL pro, Toptica) is first split into two beams by the combination of a half-wave plate (HWP1) and a polarization beam splitter (PBS1). One beam is used to lock probe laser frequency at the transition of $5S_{1/2}(F = 3) - 5P_{3/2}(F' = 4)$ by the saturation absorption spectroscopy (SAS) method. The other beam is employed to obtain the EIT spectroscopy and is injected into the center of the rubidium vapor cell. The coupling laser with 480 nm wavelength is from a frequency-doubled amplified diode laser (DLC TA-SHG pro, Toptica) and is split into two beams by the combination of HWP3 and PBS3. The reflected 480 nm beam is used to lock the frequency of the coupling laser by the EIT spectroscopy, and the transmitted beam counter-propagates and overlaps with the probe beam in the cell. Two broadband bi-convex spherical lenses with focal length of 150 mm are utilized to focus the beam and obtain higher energy densities in the interaction region. The power of probe and coupling lasers are 50 μW and 120 mW with beam diameters of 80 μm and 200 μm in the rubidium vapor cell, respectively. The corresponding Rabi frequencies are 29.7 $\times$ 2π MHz and 13.5 $\times$ 2π MHz. The cell has a length of 100 mm and 25 mm in diameter. The Rb vapor cell is at room temperature ($\sim$298 K), and the Rydberg EIT spectra are slightly affected by the temperature fluctuations in the experimental environment. Additional absorption caused by increased temperature, or metal devices for thermal regulation will cause distortions and reading errors of microwave fields. Meanwhile, the receivers operating at room temperature are easy to integrate and adapt to practical needs. After that, probe laser passed the atomic vapor is filtered by a dichroic mirror (DM), collected by a photodiode detector (PD) and recorded by a spectrum analyzer (EXA signal analyzer, Keysight) and an oscilloscope (RTO2004, Rohde & Schwarz) simultaneously. The basic vector signal generator

(B-SG) and auxiliary vector signal generator (A-SG) (SMB100A, Rohde & Schwarz) provide the B-MW and A-MW fields, respectively. A kilohertz PRBS signal, supplied by an arbitrary function generator (AFG) (3022C, Tektronix), is applied to the B-MW field by amplitude modulation. Then, these two microwave fields irradiate through two horn antennas (B-Horn and A-Horn) to the vapor cell at a distance of 50 cm to satisfy the far-field condition. The propagation direction of the microwave fields is perpendicular to both the probe and coupling beams. The probe, coupling beams, and microwave fields keep co-aligned linear polarization. The unaligned polarization among laser and microwave fields will lead to an optical pumping effect and make magnetic sublevels with $|m_j| > 1/2$ have a certain probability of population. Also, the co-aligned and linear polarization of laser and microwave fields estimates the residual EIT peaks during Aulter-Townes splitting process. The waveform of decoded PRBS signals is directly obtained on the oscilloscope by reading the output signal of the PD in real time.

3 Results and discussion

Applying the rotating-wave approximation, the Hamiltonian of the five-level system is given by [34–36]:

$$H = \frac{\hbar}{2}\begin{pmatrix} 0 & \Omega_p & 0 & 0 & 0 \\ \Omega_p & -2\Delta'_p & \Omega_c & 0 & 0 \\ 0 & \Omega_c & -2(\Delta'_p + \Delta'_c) & \Omega_{B-MW} & 0 \\ 0 & 0 & \Omega_{B-MW} & -2(\Delta'_p + \Delta'_c + \Delta_{B-MW}) & \Omega_{A-MW} \\ 0 & 0 & 0 & \Omega_{A-MW} & -2(\Delta'_p + \Delta'_c + \Delta_{B-MW} + \Delta_{A-MW}) \end{pmatrix}, \quad (1)$$

where Ω_p, Ω_c, Ω_{B-MW} and Ω_{A-MW} are the Rabi frequencies of probe, coupling, B-MW and A-MW fields, respectively, and Δ_p, Δ_c, Δ_{B-MW} and Δ_{A-MW} are their frequency detunings. Taking the Doppler effects into account, Δ_p and Δ_c are modified as $\Delta'_p = \Delta_p - 2\pi\nu/\lambda_p$ and $\Delta'_c = \Delta_c + 2\pi\nu/\lambda_c$ [34–36]. Here, ν is the velocity of the atoms, λ_p and λ_c are the wavelengths of corresponding field. Considering spontaneous radiation evolution, the atomic system satisfies the Lindblad equation [37, 38]:

$$\frac{d\rho}{dt} = -\frac{i}{\hbar}[H,\rho] + \mathcal{L}, \quad (2)$$

where $\mathcal{L}$ is the Lindblad operator considering decay terms that can be expressed as [34–36]:

$$\mathcal{L} = \begin{pmatrix} \Gamma_2\rho_{22} & -\gamma_{12}\rho_{12} & -\gamma_{13}\rho_{13} & -\gamma_{14}\rho_{14} & -\gamma_{15}\rho_{15} \\ -\gamma_{21}\rho_{21} & \Gamma_3\rho_{33} - \Gamma_2\rho_{22} & -\gamma_{23}\rho_{23} & -\gamma_{24}\rho_{24} & -\gamma_{25}\rho_{25} \\ -\gamma_{31}\rho_{31} & -\gamma_{32}\rho_{32} & \Gamma_4\rho_{44} - \Gamma_3\rho_{33} & -\gamma_{34}\rho_{34} & -\gamma_{35}\rho_{35} \\ -\gamma_{41}\rho_{41} & -\gamma_{42}\rho_{42} & -\gamma_{43}\rho_{43} & \Gamma_5\rho_{55} - \Gamma_4\rho_{44} & -\gamma_{45}\rho_{45} \\ -\gamma_{51}\rho_{51} & -\gamma_{52}\rho_{52} & -\gamma_{53}\rho_{53} & -\gamma_{54}\rho_{54} & -\Gamma_5\rho_{55} \end{pmatrix}. \quad (3)$$

Here, $\gamma_{ij} = (\Gamma_i + \Gamma_j)/2$ and Γ_i are the spontaneous decay rates of $|i>$ state. The density matrix element ρ_{ii} represents the atomic population in $|i>$ state, while ρ_{ij} stands for the coherent term between $|i>$ and $|j>$ states. The amplitude variation is deduced from the imaginary part of atomic susceptibility χ of the atoms with respect to the probe laser, which can be described as $\chi = (N|\mu_{21}|^2)/(\epsilon_0\hbar\Omega_p)\rho_{21}$. Here, N stands for atomic number density, ϵ_0 is the permittivity of free space, $\hbar$ shows the reduced Plank's constant, μ_{21}

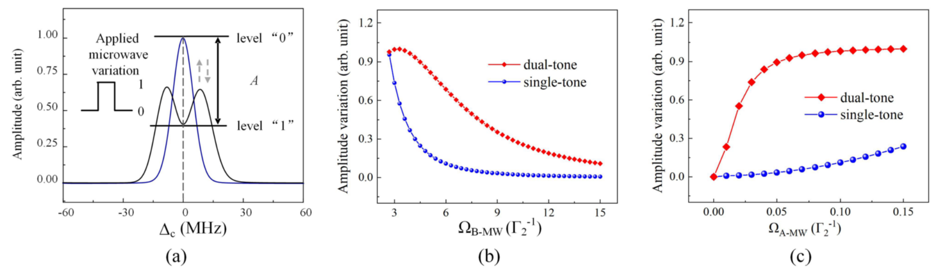

Figure 2 (a) The typical EIT (dark blue line) and AT splitting (black line) spectra. (b) The amplitude variation versus Ω_{B-MW} and (c) Ω_{A-MW} in dual-tone and single-tone microwave field cases. The amplitude variations in (b) and (c) are obtained at the resonant frequency (dash line) in (a). During the simulation, $\Gamma_1 = 0$, $\Gamma_2 = 2\pi \times 6.1$ MHz, $\Gamma_3 = 2\pi \times 0.003$ MHz, $\Gamma_4 = \Gamma_5 = 2\pi \times 0.002$ MHz, $\Omega_p = 0.79\Gamma_2$, $\Omega_c = 1.4\Gamma_2$

and ρ_{21} are the dipole momentum and density matrix element between $5S_{1/2}$ and $5P_{3/2}$ states, respectively. In a steady state, the calculation of ρ_{21} evolution can be extracted from the atomic density matrix. The vapor cell is kept at room temperature during the whole experiment, and atomic number density N stays at constant. So, the $(N|\mu_{21}|^2)/(\epsilon_0\hbar\Omega_p)$ is regarded as 1 during simulation process for simplify. The simulation of χ can be utilized to describe the atomic coherence caused EIT and the external electric field induced AT splitting spectra.

The typical EIT (dark blue line) and AT splitting (black line) spectra are shown first in Fig. 1(a). The amplitude at the resonant frequency (dash line) is the major parameter labeled as A. The EIT effect occurs when only the probe and coupling fields interact with atoms, and the A is marked as level "0" in this case. The AT splitting effect appears when a constant B-MW field is introduced and the A reduces to level "1". In particular, the A moves back and forth between "0" and "1" when the information is AM encoded in the B-MW field, and the modulated waveform can be reproduced by the optical readout method after simple NOT gate operation. The variation in A corresponds directly to the output of AM receiver. The further introduction of the A-MW field brings more obvious amplitude variation, which is directly reflected in the increment of SNR during information transmission. A quantitative simulation of amplitude variation is discussed below. The red dots and line indicate the dual-tone microwave field assisted receiver, while the blue dots and line stand for the single-tone case in the following Fig. 2(b) and (c). A quantified simulation result is presented in Fig. 2(b). The amplitude variation in the single-tone microwave field is theoretically simulated under the condition that $\Omega_p = 0.79\Gamma_2$ and $\Omega_c = 1.4\Gamma_2$. The amplitude variations of the two receivers decrease as Ω_{B-MW} increases, but the receiver with a dual-tone microwave field shows a superior amplitude variation. The best enhancement occurs at $\Omega_{B-MW} = 4.5\Gamma_2$, which provides access to the performance improvement of the Rydberg atom-based AM receiver. The dependency of the Ω_{A-MW} on the amplitude variation is shown in Fig. 2(c). The amplitude variation increases with the increment of microwave strength in both cases, while the phenomenon is more obvious with the introduction of the A-MW field. Note that the amplitude variation of atomic receiver with dual-tone microwave field increases rapidly and approaches saturation when $\Omega_{A-MW} \to 0.1\Gamma_2$.

After elaborating the mechanism theoretically, the performances of receivers with single-tone and dual-tone microwave field are tested and compared experimentally. Figure 3(a) shows the SNR of received PRBS signals as the f_{AM} increases from 0.1 kHz to

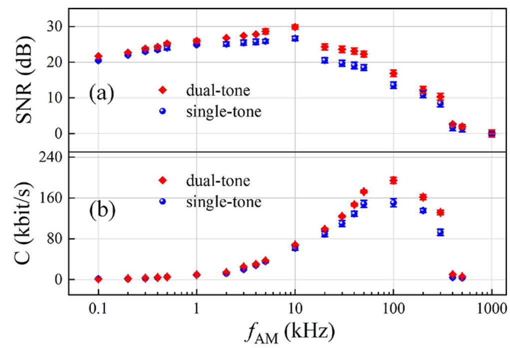

Figure 3 (a) The SNR of received signals and (b) the DTC of Rydberg atom-based receiver versus the modulation frequency (f_{AM}) for dual-tone (red dots) and single-tone (blue dots) microwave field cases. The error represents the standard deviation of three measurements

1000 kHz in dual-tone (red dots) and single-tone (blue dots) cases. The P_{B-MW} is −10 dBm, and P_{A-MW} is −15 dBm during the experiment. The SNR is obtained as the signal strength ratio at the corresponding f_{AM} to the noise when no signal is loaded. The tendencies of SNR increases from 10 kHz to 1000 kHz because atoms hardly respond once the $1/f_{AM}$ is less than the dynamic time for a steady EIT. The dynamic time is influenced by collisional relaxation, spontaneous emission, transit time broadening, etc. [39–41]. It displays that the instantaneous bandwidth of the dual-tone microwave field assisted Rydberg atom-based receiver is around 220 kHz, larger than the single-tone microwave case. The introduction of the A-MW field significantly increases the SNR over the entire range. Especially, the maximum SNR of the readout signal increases by 3 dB with the involvement of the A-MW field when the f_{AM} is 10 kHz. A large data rate is out of the responsible range of the receiver, which is limited by so-called instantaneous bandwidth. The abundant energy levels of Rydberg atoms and parallel use of multiple atomic species may give solutions to this problem.

The DTC of the readout signal is defined by the Shannon-Hartley theorem as $C = f_{AM} \times \log_2[1 + S^2/(N^2 f_{AM})]$ [1, 42]. Here, S is the measured signal in volts, and N is the voltage noise spectral density. Figure 3(b) shows the variation of DTC versus f_{AM} in the dual-tone microwave field (red dots) and the single-tone microwave field (blue dots) cases. The DTC mainly depends on the f_{AM} and significantly increases when the value ranges from 0.1 kHz to 100 kHz. The SNR becomes the major constraint from 100 kHz to 1000 kHz in contrast, and DTC decreases rapidly. The calculated DTC increases by 6.22 dB compared to the single-tone microwave case. Although the maximum DTC of the Rydberg atom-based receiver is obtained, the SNR and fidelity of the readout signal fall into a lower value. For low modulation frequencies, the data capacity has a linear dependence on the modulation frequency. For faster modulations the DTC reaches a maximum, before decreasing due to the downhill SNR caused by a finite atom-switching time. Therefore, DTC has a maximum value for f_{AM} variation, which is determined by the instantaneous bandwidth of the system and shows maximum in 100 kHz. For low modulation frequencies, the data capacity has a linear dependence on the modulation frequency. For faster modulations the DTC reaches a maximum, before decreasing due to the downhill SNR caused by a finite atom-switching time. Therefore, DTC has a maximum value for f_{AM} variation, which is determined by the instantaneous bandwidth of the system and shows maximum in 100 kHz. Therefore, f_{AM}

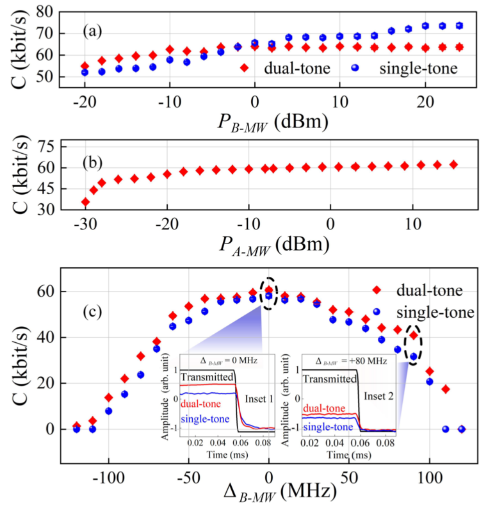

Figure 4 (a) The DTC of the Rydberg atom-based receiver versus (a) the B-MW field power $P_{B\text{–}MW}$, (b) the A-MW field power $P_{A\text{–}MW}$, and (c) the B-MW field frequency $\Delta_{B\text{–}MW}$. The error represents the standard deviation of three measurements. The transmitted and readout signals with and without the A-MW field for $\Delta_{B\text{–}MW}$ = 0 MHz in the Inset 1 and $\Delta_{B\text{–}MW}$ = +80 MHz in the Inset 2

of 10 kHz makes a trade-off between large DTC and high fidelity of Rydberg atom-based receiver.

Figure 4 shows the dependence of DTC on $P_{B\text{–}MW}$, $P_{A\text{–}MW}$, and $\Delta_{B\text{–}MW}$ of Rydberg atom-based receiver. The red and blue dots represent the measurement results in dual-tone and single-tone cases. The DTC is extracted in Fig. 4(a) as $P_{B\text{–}MW}$ increases from –20 dBm to 25 dBm, setting $P_{A\text{–}MW}$ on the –15 dBm. The DTC shows the trend that increases first and then gradually saturates in both cases. The –2 dBm is the point where relative strength goes to reverse in the two cases. The receiver with a dual-tone microwave owns a larger DTC when the $P_{B\text{–}MW}$ in the range from –20 dBm to –2 dBm. The underlying reason is that B-MW continues to increase the atom population of $54P_{3/2}$ state in both cases, leading to an increase in SNR and further in DTC. The saturation trend occurs owing to population inversion between $54P_{3/2}$ and $54S_{1/2}$ states and DTC no longer increases with $P_{B\text{–}MW}$ after reaching the threshold. The DTC inversion emerges when $P_{B\text{–}MW}$ is above –2 dBm. The major reason is the introduction of $54S_{1/2}$ state leads to the increase of DTC but decreases the saturation threshold [36]. The strength of basic microwave field larger than –2 dBm makes more atomic population at $53D_{5/2}$ state, and the effect of auxiliary microwave field turns to saturation. However, this strength range is not the suitable microwave power range for communication [16], and also corresponds to a relatively larger Rabi frequency, which leads to the Stark frequency shift and makes resonant frequency change, which is unfavorable for EIT peak detection and communication.

Figure 4(b) shows the variation of DTC with $P_{A\text{–}MW}$ increasing from –30 dBm to 15 dBm while the $P_{B\text{–}MW}$ is kept at –10 dBm. A noticeable increase is observed for the $P_{A\text{–}MW}$ ranging from –30 dBm to –20 dBm, and a saturation tendency emerges when the $P_{A\text{–}MW}$ is above –20 dBm. The number of Rydberg atoms gradually reaches the limit of atomic population reversal between $54P_{3/2}$ and $54S_{1/2}$ states in Fig. 1(a). The Rydberg atom-based receiver's maximum DTC is about 62 kbit/s at $P_{B\text{–}MW}$ = –10 dBm and $P_{A\text{–}MW}$ = –15 dBm.

Figure 5 The transmitted (black) signal and received signals with dual-tone (red) and single-tone (blue) microwave field cases

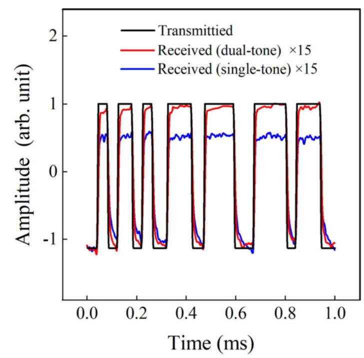

The B-MW field frequency determines the bandwidth of the Rydberg atom-based receiver, and its influence on the DTC is illustrated in Fig. 4(c). The DTC of the readout signal exhibits the maximum at resonant frequency of B-MW and gradually decreases as the frequency tunes to either blue or red detunings. The corresponding transmitted and readout signals with different B-MW field frequencies are shown in the Insets 1 and 2. Both near-resonant and off-resonant cases show higher SNR in dual-tone microwave field case. Note that the signal amplitude is more obvious, and the upper and lower edges are clearer in the case of dual-tone microwave field. The near-resonant B-MW field in the Inset 1 exhibits higher signal recovery and fidelity than the detuned case in the Inset 2.

The PRBS signal received from Rydberg atom-based receiver is compared with the original signal to evaluate the fidelity. The PRBS signal is produced in random and generated from an arbitrary waveform generator (AWG, Tektronix). The signal shows as cases of different modulation frequencies in practical application, so the width of transmitted signal is varied with time. The consistency between transmitted and received signals is kept, which shows the self-demodulation capability of atomic receivers and the potential for high-fidelity information transmission. The f_{AM} is kept at 10 kHz, P_{B-MW} is –10 dBm and P_{A-MW} is –15 dBm. The input (black) and readout signals with dual-tone microwave field (red) and the single-tone microwave (blue) cases are recorded as shown in Fig. 5. The recovery rate and signal fidelity are defined as $R_{\text{rec}} = (f_D - f_T)/f_T$ and $F_{\text{sig}} = S_T - (S_D/S_T)S_D$, respectively. The f_T and f_D represent the frequencies of transmitted and decoded signals, and S_T and S_D stand for their amplitudes, respectively [43, 44]. The R_{rec} and F_{sig} of the readout signal in the dual-tone microwave field case are 99.5% and 92.8%, while 98.9% and 80.9% in single-tone case. As a result, the enhanced features guarantees greater DTC and improved fidelity of the dual-tone microwave field assisted Rydberg atom-based receiver.

4 Conclusion

We present a Rydberg atom-based AM receiver utilizing a dual-tone microwave field in a ^{85}Rb atomic ensemble. The PRBS signal is encoded at the basic microwave field with the frequency of 14.23 GHz, then decoded by a Rydberg atom-based AM receiver. The introduction of auxiliary microwave field improves the SNR of received signals. The amplitude variations at the resonant frequency of EIT spectrum with different microwave fields involvement are investigated to provide theoretical support. The appropriate DTC of the proposed Rydberg atom-based AM receiver is about 62 kbit/s, and a 220 kHz instantaneous bandwidth is achieved. Finally, the DTC result of dual-tone microwave receiver is

6.22 dB larger than conventional single-tone microwave receiver. The dual-tone method improves Rydberg atom based receiver's response to microwave field variation, which is appropriate for not only AM scheme but also FM and PM schemes. This work takes a step closer to practical applications by opening up a new avenue for microwave communications based on Rydberg atoms.

Acknowledgements
This work is supported by the NSFC under Grants No. 62075121; Fund Program for the Scientific Activities of Selected Returned Overseas Professionals in Shanxi Province No. 2023001; and the Fund for Shanxi "1331 Project".

Data availability
The datasets used and/or analysed during the current study are available from the corresponding author on reasonable request.

Declarations

Competing interests
The authors declare no competing interests.

Author contributions
JY and TJ conceived the idea and the scheme. TJ performed the measurements. TJ and YY derived the theoretical framework and code, performed the calculations and wrote the manuscript. JY, LW contributed to reviewing, editing and assessing the results. JY, SJ, LX and LW contributed throughout, supervised the research, and provided funding. All authors reviewed the manuscript.

Received: 24 July 2023 Accepted: 13 December 2023 Published online: 02 January 2024

References

1. Meyer DH, Cox KC, Fatemi FK, Kunz PD. Digital communication with Rydberg atoms and amplitude-modulated microwave fields. Appl Phys Lett. 2018;112(21):211108. https://doi.org/10.1063/1.5028357.
2. Fancher CT, Scherer DR, John MCS, Marlow BLS. Rydberg atom electric field sensors for communications and sensing. IEEE Trans Quantum Eng. 2021;2:1–13. https://doi.org/10.1109/TQE.2021.3065227.
3. Yuan J, Yang W, Jing M, Zhang H, Jiao Y, Li W, Zhang L, Xiao L, Jia S. Quantum sensing of microwave electric fields based on Rydberg atoms. Rep Prog Phys. 2023. https://doi.org/10.1088/1361-6633/acf22f.
4. Holloway CL, Gordon JA, Jefferts S, Schwarzkopf A, Anderson DA, Miller SA, Thaicharoen N, Raithel G. Broadband Rydberg atom-based electric-field probe for SI-traceable, self-calibrated measurements. IEEE Trans Antennas Propag. 2014;62(12):6169–82. https://doi.org/10.1109/TAP.2014.2360208.
5. Artusio-Glimpse A, Simons MT, Prajapati N, Holloway CL. Modern RF measurements with hot atoms: a technology review of Rydberg atom-based radio frequency field sensors. IEEE Microw Mag. 2022;23(5):44–56. https://doi.org/10.1109/MMM.2022.3148705.
6. Lin Y-Y, She Z-Y, Chen Z-W, Li X-Z, Zhang C-X, Liao K-Y, Zhang X-D, Chen J-H, Huang W, Yan H, Zhu S-L. Terahertz receiver based on room-temperature Rydberg-atoms. Fundamental Research. 2023. https://doi.org/10.1016/j.fmre.2023.02.019.
7. Bang L, Lihua Z, Zongkai L, Zian D, Dongsheng D, Baosen S, Guangcan G. Electric field measurement and application based on Rydberg atoms. Electromagn Science. 2023;1(2):1. https://doi.org/10.23919/emsci.2022.0015.
8. Sedlacek JA, Schwettmann A, Kübler H, Löw R, Pfau T, Shaffer JP. Microwave electrometry with Rydberg atoms in a vapour cell using bright atomic resonances. Nat Phys. 2012;8(11):819–24. https://doi.org/10.1038/nphys2423.
9. Fan H, Kumar S, Sedlacek J, Kübler H, Karimkashi S, Shaffer JP. Atom based RF electric field sensing. J Phys B, At Mol Opt Phys. 2015;48(20):202001. https://doi.org/10.1088/0953-4075/48/20/202001.
10. Jing M, Hu Y, Ma J, Zhang H, Zhang L, Xiao L, Jia S. Atomic superheterodyne receiver based on microwave-dressed Rydberg spectroscopy. Nat Phys. 2020;16(9):911–5. https://doi.org/10.1038/s41567-020-0918-5.
11. Holloway C, Simons M, Haddab AH, Gordon JA, Anderson DA, Raithel G, Voran S. A multiple-band Rydberg atom-based receiver: AM/FM stereo reception. IEEE Antennas Propag Mag. 2021;63(3):63–76. https://doi.org/10.1109/MAP.2020.2976914.
12. Meyer DH, Kunz PD, Cox KC. Waveguide-coupled Rydberg spectrum analyzer from 0 to 20 GHz. Phys Rev Appl. 2021;15:014053. https://doi.org/10.1103/PhysRevApplied.15.014053.
13. Yan Y, Yuan J, Zhang L, Xiao L, Jia S, Wang L. Three-dimensional location system based on an L-shaped array of Rydberg atomic receivers. Opt Lett. 2023;48(15):3945–8. https://doi.org/10.1364/OL.496057.
14. Holloway CL, Simons MT, Haddab AH, Williams CJ, Holloway MW. A "real-time" guitar recording using Rydberg atoms and electromagnetically induced transparency: quantum physics meets music. AIP Adv. 2019;9(6):065110. https://doi.org/10.1063/1.5099036.
15. Holloway CL, Simons MT, Gordon JA, Novotny D. Detecting and receiving phase-modulated signals with a Rydberg atom-based receiver. IEEE Antennas Wirel Propag Lett. 2019;18(9):1853–7. https://doi.org/10.1109/LAWP.2019.2931450.
16. Anderson DA, Sapiro RE, Raithel G. An atomic receiver for AM and FM radio communication. IEEE Trans Antennas Propag. 2021;69(5):2455–62. https://doi.org/10.1109/TAP.2020.2987112.

17. Li S, Yuan J, Wang L. Improvement of microwave electric field measurement sensitivity via multi-carrier modulation in Rydberg atoms. Appl Sci. 2020;**10**(22). https://doi.org/10.3390/app10228110.
18. Yang K, Sun Z, Mao R, Lin Y, Liu Y, An Q, Fu Y. Wideband Rydberg atom-based receiver for amplitude modulation radio frequency communication. Chin Opt Lett. 2022;20(8):081203. https://doi.org/10.3788/COL202220.081203.
19. Yuan J, Jin T, Xiao L, Jia S, Wang L. A Rydberg atom-based receiver with amplitude modulation technique for the fifth-generation millimeter-wave wireless communication. In: IEEE antennas and wireless propagation letters. 2023. p. 1–5. https://doi.org/10.1109/LAWP.2023.3297729.
20. Song Z, Liu H, Liu X, Zhang W, Zou H, Zhang J, Qu J. Rydberg-atom-based digital communication using a continuously tunable radio-frequency carrier. Opt Express. 2019;27(6):8848–57. https://doi.org/10.1364/OE.27.008848.
21. Cai Y, Shi S, Zhou Y, Li Y, Yu J, Li W, Li L. High-sensitivity Rydberg-atom-based phase-modulation receiver for frequency-division-multiplexing communication. Phys Rev Appl. 2023;19:044079. https://doi.org/10.1103/PhysRevApplied.19.044079.
22. Simons MT, Gordon JA, Holloway CL. Simultaneous use of Cs and Rb Rydberg atoms for dipole moment assessment and RF electric field measurements via electromagnetically induced transparency. J Appl Phys. 2016;120(12):123103. https://doi.org/10.1063/1.4963106.
23. Zou H, Song Z, Mu H, Feng Z, Qu J, Wang Q. Atomic receiver by utilizing multiple radio-frequency coupling at Rydberg states of rubidium. Appl Sci. 2020;**10**(4). https://doi.org/10.3390/app10041346.
24. Otto JS, Hunter MK, Kjærgaard N, Deb AB. Data capacity scaling of a distributed Rydberg atomic receiver array. J Appl Phys. 2021;129(15):154503. https://doi.org/10.1063/5.0048415.
25. Du Y, Cong N, Wei X, Zhang X, Luo W, He J, Yang R. Realization of multiband communications using different Rydberg final states. AIP Adv. 2022;12(6):065118. https://doi.org/10.1063/5.0095780.
26. Yuan J, Zhang H, Wu C, Chen G, Wang L, Xiao L, Jia S. Creation and control of vortex-beam arrays in atomic vapor. Laser Photonics Rev. 2023;17(5):2200667. https://doi.org/10.1002/lpor.202200667.
27. Liao K, Tu H, Zhang X, Yan H, Zhu S. Rydberg atom based microwave sensing and communication. Sci Sin Phys Mech Astron. 2021;51(7):074202. https://doi.org/10.1360/SSPMA-2020-0218.
28. Fu Y, Lin Y, Wu B, An Q, Liu Y. The radio technology based on Rydberg atom. Chinese Journal of Radio Science. 2022;37(2021051):279. https://doi.org/10.12265/j.cjors.2021051.
29. Liu B, Zhang L-H, Liu Z-K, Zhang Z-Y, Zhu Z-H, Gao W, Guo G-C, Ding D-S, Shi B-S. Highly sensitive measurement of a Megahertz RF electric field with a Rydberg-atom sensor. Phys Rev Appl. 2022;18:014045. https://doi.org/10.1103/PhysRevApplied.18.014045.
30. Jiao Y, Han X, Fan J, Raithel G, Zhao J, Jia S. Atom-based receiver for amplitude-modulated baseband signals in high-frequency radio communication. Appl Phys Express. 2019;12(12):126002. https://doi.org/10.7567/1882-0786/ab5463.
31. Li H, Hu J, Bai J, Shi M, Jiao Y, Zhao J, Jia S. Rydberg atom-based AM receiver with a weak continuous frequency carrier. Opt Express. 2022;30(8):13522–9. https://doi.org/10.1364/OE.454873.
32. Meyer DH, Hill JC, Kunz PD, Cox KC. Simultaneous multiband demodulation using a Rydberg atomic sensor. Phys Rev Appl. 2023;19:014025. https://doi.org/10.1103/PhysRevApplied.19.014025.
33. Liu Z-K, Zhang L-H, Liu B, Zhang Z-Y, Guo G-C, Ding D-S, Shi B-S. Deep learning enhanced Rydberg multifrequency microwave recognition. Nat Commun. 2022;13(1):1997. https://doi.org/10.1038/s41467-022-29686-7.
34. Jia F-D, Liu X-B, Mei J, Yu Y-H, Zhang H-Y, Lin Z-Q, Dong H-Y, Zhang J, Xie F, Zhong Z-P. Span shift and extension of quantum microwave electrometry with Rydberg atoms dressed by an auxiliary microwave field. Phys Rev A. 2021;103:063113. https://doi.org/10.1103/PhysRevA.103.063113.
35. Robinson AK, Artusio-Glimpse AB, Simons MT, Holloway CL. Atomic spectra in a six-level scheme for electromagnetically induced transparency and Autler-Townes splitting in Rydberg atoms. Phys Rev A. 2021;103:023704. https://doi.org/10.1103/PhysRevA.103.023704.
36. Jin T, Li S, Yuan J, Wang L, Xiao L, Jia S. Coherent population transfer of Rydberg atoms in a dual-microwave driven five-level configuration. Opt Commun. 2022;522:128603. https://doi.org/10.1016/j.optcom.2022.128603.
37. Osterwalder A, Merkt F. Using high Rydberg states as electric field sensors. Phys Rev Lett. 1999;82:1831–4. https://doi.org/10.1103/PhysRevLett.82.1831.
38. Berweger S, Prajapati N, Artusio-Glimpse AB, Rotunno AP, Brown R, Holloway CL, Simons MT, Imhof E, Jefferts SR, Kayim BN, Viray MA, Wyllie R, Sawyer BC, Walker TG. Rydberg-state engineering: investigations of tuning schemes for continuous frequency sensing. Phys Rev Appl. 2023;19:044049. https://doi.org/10.1103/PhysRevApplied.19.044049.
39. Bussey LW, Winterburn A, Menchetti M, Burton F, Whitley T. Rydberg RF receiver operation to track RF signal fading and frequency drift. J Lightwave Technol. 2021;39(24):7813–20. https://doi.org/10.1109/JLT.2021.3098348.
40. Prajapati N, Rotunno AP, Berweger S, Simons MT, Artusio-Glimpse AB, Voran SD, Holloway CL. TV and video game streaming with a quantum receiver: a study on a Rydberg atom-based receiver's bandwidth and reception clarity. AVS Quantum Sci. 2022;4(3):035001. https://doi.org/10.1116/5.0098057.
41. You S, Cai M, Zhang H, Xu Z, Liu H. Exclusive effect in Rydberg atom-based multi-band microwave communication. Photonics. 2023;**10**(3). https://doi.org/10.3390/photonics10030328.
42. Bohaichuk SM, Booth D, Nickerson K, Tai H, Shaffer JP. Origins of Rydberg-atom electrometer transient response and its impact on radio-frequency pulse sensing. Phys Rev Appl. 2022;18:034030. https://doi.org/10.1103/PhysRevApplied.18.034030.
43. Tse D, Viswanath P. Fundamentals of wireless communication. London: Cambridge University press; 2005.
44. Goldsmith A. Wireless communications. London: Cambridge University press; 2005.

Publisher's Note